AJNR

Correlation between Cranial Nerve Microstructural Characteristics and Vestibular Schwannoma Tumor Volume

A.M. Halawani, S. Tohyama, P.S.-P. Hung, B. Behan, M. Bernstein, S. Kalia, G. Zadeh, M. Cusimano, M. Schwartz, F. Gentili, D.J. Mikulis, N.J. Laperriere and M. Hodaie

AJNR Am J Neuroradiol 2021, 42 (10) 1853-1858
doi: https://doi.org/10.3174/ajnr.A7257
http://www.ajnr.org/content/42/10/1853

Correlation between Cranial Nerve Microstructural Characteristics and Vestibular Schwannoma Tumor Volume

A.M. Halawani, S. Tohyama, P.S.-P. Hung, B. Behan, M. Bernstein, S. Kalia, G. Zadeh, M. Cusimano, M. Schwartz, F. Gentili, D.J. Mikulis, N.J. Laperriere, and M. Hodaie

ABSTRACT

BACKGROUND AND PURPOSE: Vestibular schwannomas are common cerebellopontine angle tumors arising from the vestibulocochlear nerve and can result in cranial nerve dysfunction. Conventional MR imaging does not provide information that could correlate with cranial nerve compression symptoms of hearing loss or imbalance. We used multitensor tractography to evaluate the relationship between the WM microstructural properties of cranial nerves and tumor volume in a cohort of patients with vestibular schwannomas.

MATERIALS AND METHODS: A retrospective study was performed in 258 patients with vestibular schwannomas treated at the Gamma Knife clinic at Toronto Western Hospital between 2014 and 2018. 3T MR images were analyzed in 160 surgically naïve patients with unilateral vestibular schwannomas. Multitensor tractography was used to extract DTI-derived metrics (fractional anisotropy and radial, axial, and mean diffusivities of the bilateral facial and vestibulocochlear nerves [cranial nerves VII/VIII]). ROIs were placed in the transition between cisternal and intracanalicular segments, and images were analyzed using the eXtended Streamline Tractography reconstruction method. Diffusion metrics were correlated with 3D tumor volume derived from the Gamma Knife clinic.

RESULTS: DTI analyses revealed significantly higher fractional anisotropy values and a reduction in axial diffusivity, radial diffusivity, and mean diffusivity (all $P < .001$) within the affected cranial nerves VII and VIII compared with unaffected side. All specific diffusivities (axial, radial, and mean diffusivity) demonstrated an inverse correlation with tumor volume (axial, radial, and mean diffusivity, $P < .01$).

CONCLUSIONS: Multitensor tractography allows the quantification of cranial nerve VII and VIII WM microstructural alterations in patients with vestibular schwannomas. Our findings support the hypothesis that tumor volume may cause microstructural alterations of the affected cranial nerves VII and VIII. This type of advanced imaging may represent a possible avenue to correlate diffusivities with cranial nerve function.

ABBREVIATIONS: AD = axial diffusivity; CN = cranial nerve; FA = fractional anisotropy; IC = intracanalicular; MD = mean diffusivity; MTT = multitensor tractography; RD = radial diffusivity; VS = vestibular schwannoma

Vestibular schwannomas (VSs) are slow-growing tumors of myelin-forming cells that originate from the vestibulocochlear nerve. The tumor commonly originates near the vestibular ganglion at the junction of the central and peripheral myelin near the porus of the auditory meatus but can be found anywhere along the nerve from the internal auditory canal to the terminal ends of the vestibulocochlear nerve (cranial nerve [CN] VIII) within the vestibule, cochlea, or semicircular canals.[1-4] VSs typically grow within a capsule and remain peripherally attached to the parent vestibulocochlear nerve, which is splayed over the surface of the tumor.[5,6] As these tumors grow, they can affect hearing status and balance, resulting in asymmetric hearing loss, tinnitus, and dizziness. Further growth can result in mass effect on the facial nerve, trigeminal nerve, or, occasionally, the brain stem, resulting in variable symptoms.

Received August 7, 2020; accepted after revision May 28, 2021.

From the Division of Brain Imaging and Behaviour–Systems Neuroscience (A.M.H., S.T., P.S.-P.H., D.J.M., M.H.), Krembil Research Institute, Division of Neuroradiology (A.M.H., D.J.M.), Joint Department of Medical Imaging, and Division of Neurosurgery (M.B., S.K., F.G., M.H.), Krembil Neuroscience Centre, Toronto Western Hospital, University Health Network, Toronto, Ontario, Canada; Institute of Medical Science, (S.T., P.S.-P.H., M.H.), Departments of Surgery (M.B., S.K., G.Z., M.C., F.G., M.H.), Medical Imaging (A.M.H., D.J.M.), Faculty of Medicine, and Radiation Oncology (N.J.L.), University of Toronto, Toronto, Ontario, Canada; Ontario Brain Institute (B.B.), Toronto, Ontario, Canada; Division of Neurosurgery (M.C.), St Michael's Hospital, Unity Health, Toronto, Ontario, Canada; Division of Neurosurgery (M.S.), Sunnybrook Health Sciences Centre, Toronto, Ontario, Canada; The Arthur and Sonia Labatt Brain Tumor Research Centre (G.Z.), Hospital for Sick Children, Toronto, Ontario, Canada; and Division of Radiation Oncology (N.J.L.), Princess Margaret Hospital, University Health Network, Toronto, Ontario, Canada.

Please address correspondence to Mojgan Hodaie, MD, MSc, FRCS(C), Toronto Western Hospital, Division of Neurosurgery, 399 Bathurst St, 4W W-443, Toronto, ON, Canada M5T 2S8; e-mail: mojgan.hodaie@uhn.ca; @mhodaie

http://dx.doi.org/10.3174/ajnr.A7257

DWI is a neuroimaging technique focused on the measurement of tissue water diffusion by applying special diffusion-encoding gradients.[7] In white matter tracts and CNs, the architecture of the axonal bundles with their myelin sheath facilitates water molecule motion along rather than transverse to the direction of the bundle. When multiple diffusion gradients are applied, the diffusion tensor within each voxel can be calculated, allowing visualization of CNs including CNs VII and VIII.[8] CNs VII and VIII will be, hereafter, grouped together as 1 entity—the facial/vestibular complex (CN VII/VIII)—because both fibers tend to be closely aligned with one another in diffusion-weighted scans.[9] DTI has been investigated for studying the structural connectivity and the quantitative assessment of diffusion restriction as a marker of the neuronal microstructural integrity.[10,11] Single-tensor diffusion tractography assumes that in each voxel, there is 1 representative fiber orientation. This assumption does not hold in areas of high crossing fibers where the orientation of the fibers is not unique and multiple orientations may exist simultaneously. Multitensor tractography (MTT) imaging can estimate ≥2 tensors within a voxel and improves fiber orientation in these regions. Behan et al[9] reported that the eXtended Streamline Tractography reconstruction method is effective in producing more detailed projections of CN VII/VIII than other reconstruction methods. Other publications have proved the efficacy of DTI on CN VII/VIII tractography[8,12-16] and preoperative facial nerve identification.[17-28]

The role of DTI in the study of CNs is increasing,[29-31] and WM microstructural alternations of the auditory neural pathway in patients with VS have been evaluated,[32,33] though not the cisternal segment of the vestibulocochlear nerve, chiefly due to the technical challenges this represents.

This study aimed to identify the microstructural alternations of the cisternal vestibulocochlear nerve and its association with tumor volume in patients with VS. Because a large VS can cause mechanical compression to surrounding structures, we hypothesized that the tumor can cause microstructural alternations along the distal cisternal/intracanalicular (IC) vestibulocochlear nerve and that tumor volume will correlate with microstructural alternations in the affected CN VII/VIII.

MATERIALS AND METHODS

Participants

A retrospective chart review was performed for all patients with VS treated with gamma knife radiosurgery between January 1, 2014, and December 31, 2018, after approval by the institutional review board at Toronto Western Hospital. Overall, 258 patients with VS were enrolled. After we excluded patients with bilateral VSs (9 patients), prior surgical treatment (partial surgical resection or gamma knife radiosurgery, 23 patients), nonavailability of DTI studies (52 patients), and additional technical difficulties related to eddy current and motion correction (12 patients), a total of 162 patients were enrolled. Two other patients with outliers were identified (one had a huge tumor volume compared with other subjects, and the other had marked motion on the clinical DWI sequence), both resulting in improper tract reconstruction, and were also excluded. Thus, a total of 160 patients were included in our DTI analysis. The analysis focused solely on images obtained before gamma knife radiosurgery treatment.

Tumor Volume

We evaluated tumor size using volumetric measurements. The semiautomatic segmentation function was used with 1-mm-section FIESTA MR images for volumetric measurements. Manual contouring was performed by a trained assistant to delineate the tumor and measure the tumor volume. The tumor volume was measured in milliliters (mL). In all subjects, treatment with gamma knife radiosurgery commenced within 21 days after MR images were acquired.

Image Acquisition

Images were acquired with 3T MR imaging (Signa; GE Healthcare) with an 8-channel phased-array head coil following our routine clinical imaging protocol. DWI scans (60 directions, spin-echo EPI sequence, 1 B_0, b = 1000 s/mm^2, one excitation, array spatial sensitivity encoding technique, voxel size = 0.94 × 0.94 × 3 mm^3, matrix = 256 × 256, TR = 12,000 ms, TE = 86.4 ms, flip angle = 90°, FOV = 24 × 24 cm) were acquired. High-resolution 3D T1-weighted anatomic fast-spoiled gradient recalled and T2-weighted FIESTA scans were obtained for coregistration with MTT images using an inversion recovery fast-spoiled gradient recalled sequence.

Image Processing and Registration

Following eddy current and motion correction with FSL (http://www.fmrib.ox.ac.uk/fsl), the diffusion tensor estimation and derivation of scalar maps (ie, fractional anisotropy [FA], mean diffusivity [MD], radial diffusivity [RD], and axial diffusivity [AD]) were extracted manually using 3D Slicer, Version 4.3 (National Alliance for Medical Image Computing; http://www.slicer.org).[34] The T1-weighted anatomic image was linearly coregistered on the DTI examination with respect to the following landmarks: basilar artery, vertebral arteries, ventral brain stem, tumor configuration, internal auditory canals, fourth ventricle, and cerebellar surface.

Microstructural Analysis

ROIs were placed on the proximal IC segments on both sides where the CNs can be most easily identified anatomically. All seeds were mapped to incorporate a cross-section of the CN of interest and did not exceed 25 mm^2. The ROIs were reconstructed by eXtended Streamline Tractography methods, traced CN VII/VIII tracts were further analyzed on the basis of fiber orientation, and then diffusivity measurements were evaluated. ROIs were used for both tractography construction and diffusivity measurements. The reconstructed tracts were examined in a blinded fashion by a subcommittee of the authors (S.T., P.S.-P.H., and A.M.H.). Two patients with improper tract reconstruction were excluded by consensus among this group.

We defined the CN "vulnerable zone" as the transition between the cisternal and IC segments, which is an anatomic area with increased mechanical compression by the tumor. For the unaffected side, we defined the same vulnerable zone where the nerves were seen to travel in close proximity and were difficult to differentiate anatomically (Fig 1).

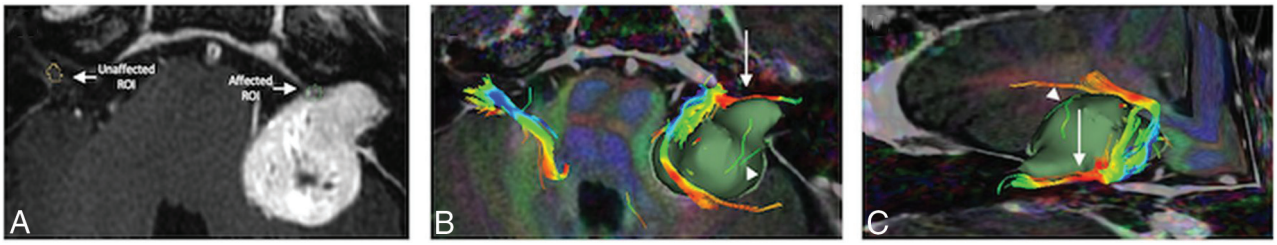

FIG 1. TI-weighted anatomic image (*A*) and 2 fused DTI/TI-weighted images (*B* and *C*) with superimposed representation of tumor volume (green) used to locate the ROIs within the distal cisternal/IC segments (*A*) and to demonstrate the extracted CN VII/VIII tracts (*B* and *C*). Note the detailed correspondence of the tumor and its effect on CN VII/VIII (*white arrows*). The CN VII/VIII can be seen sweeping anterior to the tumor. Also, note scattered, disconnected fibers that are not corresponding to CN configuration in space. These fibers were disregarded anatomically (*arrowheads*).

Criteria of CN Tractography Assessment

The criteria of CN tractography assessment were the following:

1) Anatomic accuracy: we ensured that there was an appropriate representation of the generated tracts in correlation with the CNs on the anatomic T1 image (fast-spoiled gradient recalled) and T2 image (FIESTA) sequences.

2) Delineation of the tumor mass effect on the CNs: special consideration was given to tumor fiber contamination, especially in large tumors where it was difficult to identify the exact anatomy of the affected CNs.

It may be difficult to differentiate the CN VII/VIII on the unaffected side, given the small size of the nerves and their close proximity to each other. Conventional T1-weighted images were used as a guide to identify the orientation and course of both nerves, and tractography reconstruction was easier to obtain compared with the affected side. On the affected side, the ROI was placed at our defined vulnerable zone, where the tumor caused the maximum compression on the nerve against adjacent structures. This placement provides the advantage of a consistent ROI definition for every patient. We avoided an intracanalicular ROI definition because the canal can be narrow with surrounding bone.

Statistical Analysis

All analyses were conducted in SPSS, Version 22.0 (IBM). Multiple comparisons were corrected for all 4 diffusivity metrics for each separate analysis using false discovery rate correction. Statistical significance was determined at $P < .01$ or false discovery rate–corrected P value (q) $< .01$ when adjustments were necessary for multiple comparisons. The average microstructural diffusivity differences between the affected and unaffected CN VII/VIII for each patient were evaluated using paired-sample t tests. Continuous variables were summarized as mean (SD). We used the Kolmogorov-Smirnov test to assess normality and the Spearman rank correlation to assess the relationship between DTI metrics and tumor volume.

RESULTS

Clinical Characteristics

We identified 160 surgically naïve patients with unilateral VSs (68 men and 92 women; mean age, 64.2 [SD, 13] years; range, 28–94 years; median, 64.1 years). On clinical assessment, 79 patients (32 men and 47 women) had both tinnitus and sensorineural hearing loss, 33 patients (15 men and 18 women) had isolated sensorineural hearing loss, 7 patients (6 men and 1 woman) had isolated tinnitus, 3 patients (1 man and 2 women) had sensorineural hearing loss and trigeminal neuralgia pain, and 1 patient (1 woman) had isolated trigeminal neuralgia pain. Unfortunately, we could not access the electronic health records of 37 patients.

Tumor Morphology

Tumor volume ranged from 0.2 to 9.5 mL (mean, 2.3 [SD, 0.6] mL; median, 1.3 mL). Sixty-nine patients had a right-sided tumor, and 91 patients had a left-sided tumor. In all 160 patients, 17 patients had a VS primarily in the cerebellopontine angle, 10 patients had an isolated intracanalicular vestibular schwannoma, and 133 patients had both cerebellopontine angle and IC tumors.

On conventional imaging, the tumor resulted in a significant disruption of the proximal cisternal CN VIII nerve, and it was difficult to trace along the bulk of tumor. The CN VIII fibers distal to the tumor were visualized occasionally. The morphologic assessment is challenging in large tumors with brain stem compression, due to significant anatomic distortion. On MTT, most of the extracted CN VII/VIII tracts had an anterior or anteroinferior relationship to the tumor; the fibers were seen sweeping anterior to the tumor, resulting in color changes on the FA map (Fig 1).

Diffusion Metrics Changes

We found a statistically significant increase in the average FA ($P < .001$, q $< .001$) and significant reduction in the average specific diffusivities (AD: $P < .001$, q $< .001$; RD: $P < .001$, q $< .001$; and MD: $P < .001$, q $< .001$) in all patients with VS at the affected CN VII/VIII compared with the unaffected side (Fig 2). The quantitative summary data of FA and diffusivities are summarized in the Table.

Correlation Analysis

The results of the Pearson correlation coefficient test and the Spearman ρ showed a small-but-significant negative linear relationship between the tumor volume and the specific diffusivities: AD (r_s =158 = −0.3, $P = .001$, q = 0.004), RD (r_s = 158 = −0.24, $P = .004$, q = 0.008), and MD (r_s = 158 = −0.23, $P = .007$, q = 0.009). FA values did not show a statistically significant correlation

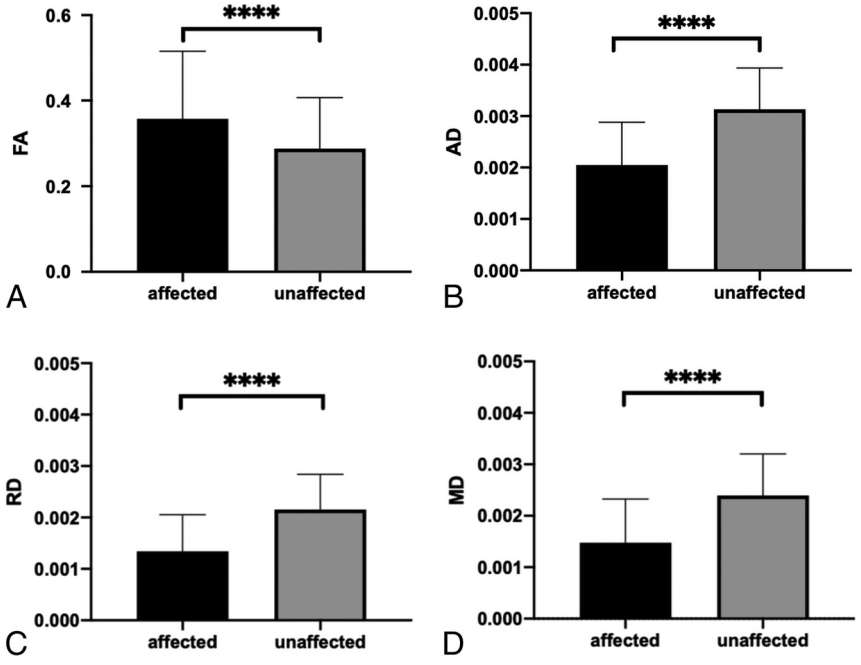

FIG 2. Microstructural properties of the CN VII/VIII in patients with VS. The averaged mean value of the diffusivity measurements in all patients with VS that demonstrate abnormal WM microstructural changes in their VII/VIII nerves (*four asterisks* indicate $P < .0001$ false discovery rate–corrected). DTI-derived values ± standard error of the mean of affected (*black bars*) and unaffected (*gray bars*) sides. Compared with the unaffected side, patients had significantly higher FA (*A*) and lower AD (*B*), RD (*C*), and MD (*D*) on their affected side. Diffusion is in square millimeters/second.

The mean, median, and range values for averaged FA and diffusivity

	Mean	Median	Range
FA (mm^2/s)			
Affected	0.357	0.332	0.108–0.722
Nonaffected	0.287	0.256	0.114–0.746
AD (mm^2/s)			
Affected	0.002	0.002	0.001–0.006
Nonaffected	0.003	0.003	0.001–0.005
RD (mm^2/s)			
Affected	0.001	0.001	0–0.004
Nonaffected	0.002	0.002	0–0.003
MD (mm^2/s)			
Affected	0.001	0.001	0–0.005
Nonaffected	0.002	0.002	0–0.004

with the tumor volume ($r_s = 158 = -0.02$, $P = .870$, $q = 0.87$) (Fig 3).

DISCUSSION

In the present study, we defined the WM microstructural alteration on the cisternal segment of CN VII/VIII in surgically naïve patients with VS. This study is the first to describe the WM microstructural abnormality characterized by higher FA and lower AD, RD, and MD in the vulnerable zone of the affected side compared with the unaffected side. Furthermore, all specific diffusivities (AD, RD, and MD) demonstrated an inverse correlation with tumor volume but not FA. These results are in line with our hypothesis that tumors cause microstructural changes which are, in turn, related to tumor volume. While these metrics are not obtained from conventional MR images, MTT is a sensitive tool that provides quantitative diffusion measures and tissue fiber orientation to help develop a better understanding of hearing impairment pathophysiology in patients with VS. It may provide a useful surrogate to measure the alterations in the CN VII/VIII as a result of tumor compression.

The quantitative diffusivity metrics are calculated from the tensors. These maps are generated by mapping the directional components of the major eigenvectors in the $\lambda 1$, $\lambda 2$, and $\lambda 3$ planes. AD indicates diffusion along with the main axis of the ellipsoid, RD is a measure of diffusion along the other 2 orthogonal directions, and MD is equivalent to the average of the eigenvalues.[35,36] These metrics (AD, RD, and MD) have been linked to pathophysiologic mechanisms such as axonal degeneration,[37] demyelination,[38,39] and neuroinflammation.[35]

Because AD is sensitive to axonal integrity, the present study showed a lower AD value in the cisternal segment of the affected vestibulocochlear nerve. This may relate to axonal damage secondary to Wallerian degeneration,[40-42] focal misalignment of neurofilaments, and/or beading in injured axons, which may also result in the reduction of MD.[43-46] Alternatively, the lower AD value can be seen in the assumed increased tumor cellular density in the extracellular matrix.[47,48]

The increase in FA and reduction of MD may be other reliable indicators of damaged fiber integrity, but these are dependent on the brain region and cellular basis.[49,50] Several factors, such as an increase in myelination, microscopic deficits of axonal structures, decreases in axonal diameter, and packing density may contribute to the higher FA.

Although in previous studies, the RD increased in cases of dysmyelination or demyelination,[38,51] we report a reduction on RD value in the affected CN VII/VIII. As the RD indicates diffusion along the two minor orthogonal directions of the traced nerve bundles, we assume that the lower value found in our study may represent a reduction in this cross-sectional area secondary to compression and/or nerve bundle atrophy.

We found that a small inverse relationship exists between the tumor volume and WM microstructural alteration, with a significant degree of agreement. This relationship supports our hypothesis that the tumor volume may cause microstructural alterations in the vulnerable zone of the ipsilateral CN VII/VIII, and it seems to be in line with past studies that confirmed that nerve compression is not the only cause of hearing loss in patients with VS.[52]

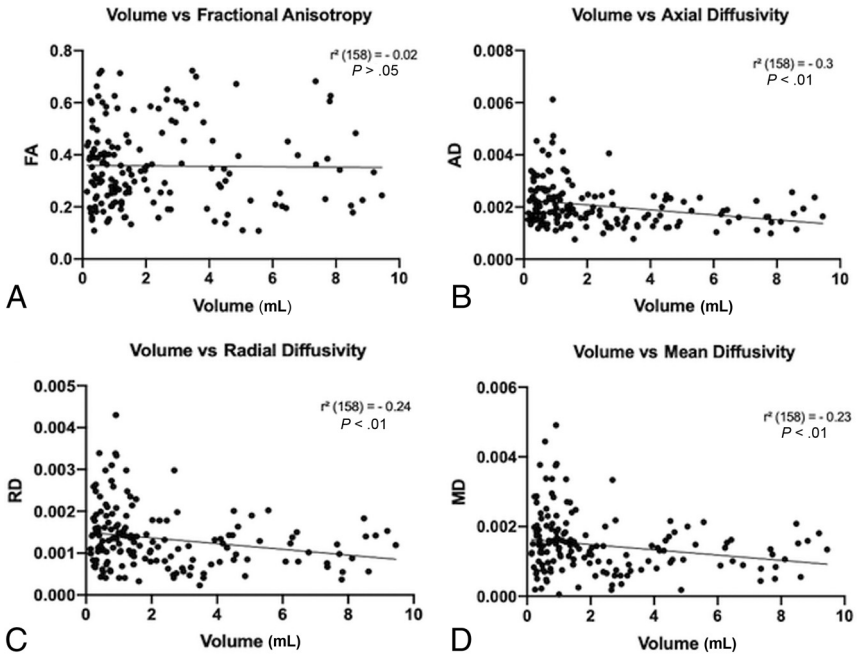

FIG 3. Scatterplots of the relationship between tumor volume and microstructural properties in the affected CNs VII/VIII. A weak-but-significant inverse relationship exists between the tumor volume and the specific diffusivities: axial diffusivity (*B*), radial diffusivity (*C*), and mean diffusivity (*D*), but not with FA (*A*) (significant at $P < .01$; false discovery rate–corrected). Diffusion is in square millimeters/second.

There are some limitations to the current study. The retrospective design made it difficult to acquire patient charts and record all clinical variables. The voxel size for the DWI scan is not equal across all 3 dimensions and is still considered larger than the dimensions of the axons, which may also be inhomogeneous due to tumor distortion. We assume this might be the cause of these variable metric abnormalities. In the future, further studies may focus on WM microstructural alterations along the auditory neural pathway aiming for better understanding and explanation of hearing impairment in this patient group using this noninvasive neuroimaging tool. Moreover, this study paves the way for more studies on posttreatment response prediction to aid in high-risk group identification and clinical prognostication.

CONCLUSIONS

This was a large cohort study that defined the WM microstructural signature of the cisternal CN VII/VIII in surgically naïve patients with VS. We evaluated microstructural alternations in correlation to tumor size volume in the affected vestibulocochlear nerve. Our observations indicate that MTT is a powerful, noninvasive tool that may play a role in the future in treatment planning and clinical decision-making.

ACKNOWLEDGMENTS

We thank Alborz Noorani and Powell Chu for expert technical assistance.

Disclosures: Peter Shih-Ping Hung—*UNRELATED*: *Employment*: University of Toronto. Brendan Behan—*UNRELATED*: *Employment*: Ontario Brain Institute. Suneil Kalia—*UNRELATED*: *Consultancy*: Medtronic; *Grants/Grants Pending*: Canadian Institutes of Health Research. Gelareh Zadeh—*UNRELATED*: *Employment*: University Health Network, Princess Margaret Cancer Center.

REFERENCES

1. Karlan MS, Basek M, Potter GB. **Intracochlear neurilemoma.** *Arch Otolaryngol* 1972;96:573–75 CrossRef Medline
2. Hoshino T, Ishii D. **Intralabyrinthine neurilemmoma.** *ORL J Otorhinolaryngol Relat Spec* 1972;34:117–23 CrossRef Medline
3. Kennedy RJ, Shelton C, Salzman KL, et al. **Intralabyrinthine schwannomas: diagnosis, management, and a new classification system.** *Otol Neurotol* 2004;25:160–67 CrossRef Medline
4. Salzman KL, Childs AM, Davidson HC, et al. **Intralabyrinthine schwannomas: imaging diagnosis and classification.** *AJNR Am J Neuroradiol* 2012;33:104–09 CrossRef Medline
5. Wippold FJ, Lubner M, Perrin RJ, et al. **Neuropathology for the neuroradiologist: Antoni A and Antoni B tissue patterns.** *AJNR Am J Neuroradiol* 2007;28:1633–38 CrossRef Medline
6. Coons SW. **Pathology of schwannomas of the eighth cranial nerve.** *Operative Techniques in Neurosurgery* 2001;4:53–57 CrossRef
7. Johansen-Berg H, Rushworth MF. **Using diffusion imaging to study human connectional anatomy.** *Annu Rev Neurosci* 2009;32:75–94 CrossRef Medline
8. Chen DQ, Quan J, Guha A, et al. **Three-dimensional in vivo modeling of vestibular schwannomas and surrounding cranial nerves with diffusion imaging tractography.** *Neurosurgery* 2011;68:1077–83 CrossRef Medline
9. Behan B, Chen DQ, Sammartino F, et al. **Comparison of diffusion-weighted MRI reconstruction methods for visualization of cranial nerves in posterior fossa surgery.** *Front Neurosci* 2017;11:554 CrossRef Medline
10. Mori S, Zhang J. **Principles of diffusion tensor imaging and its applications to basic neuroscience research.** *Neuron* 2006;51:527–39 CrossRef Medline
11. Kumar M, Rathore RK, Srivastava A, et al. **Correlation of diffusion tensor imaging metrics with neurocognitive function in Chiari 1 malformation.** *World Neurosurg* 2011;76:189–94 CrossRef Medline
12. Hodaie M, Quan J, Chen DQ. **In vivo visualization of cranial nerve pathways in humans using diffusion-based tractography.** *Neurosurgery* 2010;66:788–96 CrossRef Medline
13. Zolal A, Juratli TA, Podlesek D, et al. **Probabilistic tractography of the cranial nerves in vestibular schwannoma.** *World Neurosurg* 2017;107:47–53 CrossRef Medline
14. Yoshino M, Kin T, Ito A, et al. **Diffusion tensor tractography of normal facial and vestibulocochlear nerves.** *Int J Comput Assist Radiol Surg* 2015;10:383–92 CrossRef Medline
15. Yoshino M, Abhinav K, Yeh FC, et al. **Visualization of cranial nerves using high-definition fiber tractography.** *Neurosurgery* 2016;79:146–65 CrossRef Medline
16. Cauley KA, Filippi CG. **Diffusion-tensor imaging of small nerve bundles: cranial nerves, peripheral nerves, distal spinal cord, and lumbar nerve roots—clinical applications.** *AJR Am J Roentgenol* 2013;201:326–35 CrossRef Medline

17. Yoshino M, Kin T, Ito A, et al. **Combined use of diffusion tensor tractography and multifused contrast-enhanced FIESTA for predicting facial and cochlear nerve positions in relation to vestibular schwannoma.** *J Neurosurg* 2015;123:1480–88 CrossRef Medline
18. Mastronardi L, Cacciotti G, Roperto R, et al. **Position and course of facial nerve and postoperative facial nerve results in vestibular schwannoma microsurgery.** *World Neurosurg* 2016;94:174–80 CrossRef Medline
19. Zhang Y, Mao Z, Wei P, et al. **Preoperative prediction of location and shape of facial nerve in patients with large vestibular schwannomas using diffusion tensor imaging–based fiber tracking.** *World Neurosurg* 2017;99:70–78 CrossRef Medline
20. Choi KS, Kim MS, Kwon HG, et al. **Preoperative identification of facial nerve in vestibular schwannomas surgery using diffusion tensor tractography.** *J Korean Neurosurg Soc* 2014;56:11–15 CrossRef Medline
21. Gerganov VM, Giordano M, Samii M, et al. **Diffusion tensor imaging-based fiber tracking for prediction of the position of the facial nerve in relation to large vestibular schwannomas: clinical article.** *J Neurosurg* 2011;115:1087–93 CrossRef Medline
22. Song F, Hou Y, Sun G, et al. **In vivo visualization of the facial nerve in patients with acoustic neuroma using diffusion tensor imaging-based fiber tracking.** *J Neurosurg* 2016;125:787–94 CrossRef Medline
23. Li H, Wang L, Hao S, et al. **Identification of the facial nerve in relation to vestibular schwannoma using preoperative diffusion tensor tractography and intraoperative tractography-integrated neuronavigation system.** *World Neurosurg* 2017;107:669–77 CrossRef Medline
24. Churi ON, Gupta S, Misra BK. **Correlation of preoperative cranial nerve diffusion tensor tractography with intraoperative findings in surgery of cerebellopontine angle tumors.** *World Neurosurg* 2019;127:e509–16 CrossRef Medline
25. d'Almeida GN, Marques LS, Escada P, et al. **Diffusion tensor tractography in the preoperative precise identification of the course of facial nerve in a meningioma of the cerebellopontine angle: technical implications.** *Interdiscip Neurosurg* 2017;9:58–60 CrossRef
26. Taoka T, Hirabayashi H, Nakagawa H, et al. **Displacement of the facial nerve course by vestibular schwannoma: preoperative visualization using diffusion tensor tractography.** *J Magn Reson Imaging* 2006;24:1005–10 CrossRef Medline
27. Yoshino M, Kin T, Ito A, et al. **Feasibility of diffusion tensor tractography for preoperative prediction of the location of the facial and vestibulocochlear nerves in relation to vestibular schwannoma.** *Acta Neurochir (Wien)* 2015;157:939–46 CrossRef Medline
28. Wei PH, Qi ZG, Chen G, et al. **Identification of cranial nerves near large vestibular schwannomas using superselective diffusion tensor tractography: experience with 23 cases.** *Acta Neurochir (Wien)* 2015;157:1239–49 CrossRef Medline
29. Shapey J, Vos SB, Vercauteren T, et al. **Clinical applications for diffusion MRI and tractography of cranial nerves within the posterior fossa: a systematic review.** *Front Neurosci* 2019;13:23 CrossRef Medline
30. Jacquesson T, Frindel C, Kocevar G, et al. **Overcoming challenges of cranial nerve tractography: a targeted review.** *Clin Neurosurg* 2019;84:313–25 CrossRef Medline
31. Ma J, Su S, Yue S, et al. **Preoperative visualization of cranial nerves in skull base tumor surgery using diffusion tensor imaging technology.** *Turk Neurosurg* 2016;26:805–12 CrossRef Medline
32. Rueckriegel SM, Homola GA, Hummel M, et al. **Probabilistic fiber-tracking reveals degeneration of the contralateral auditory pathway in patients with vestibular schwannoma.** *AJNR Am J Neuroradiol* 2016;37:1610–16 CrossRef Medline
33. Kurtcan S, Hatiboglu MA, Alkan A, et al. **Evaluation of auditory pathways using DTI in patients treated with gamma knife radiosurgery for acoustic neuroma: a preliminary report.** *Clin Neuroradiol* 2018;28:377–83 CrossRef Medline
34. Fedorov A, Beichel R, Kalpathy-Cramer J, et al. **3D slicer as an image computing platform for the quantitative imaging network.** *Magn Reson Imaging* 2012;30:1323–41 CrossRef Medline
35. Alexander AL, Lee JE, Lazar M, et al. **Diffusion tensor imaging of the brain.** *Neurotherapeutics* 2007;4:316–29 CrossRef Medline
36. Beppu T, Inoue T, Shibata Y, et al. **Measurement of fractional anisotropy using diffusion tensor MRI in supratentorial astrocytic tumors.** *J Neurooncol* 2003;63:109–16 CrossRef Medline
37. Song SK, Sun SW, Ju WK, et al. **Diffusion tensor imaging detects and differentiates axon and myelin degeneration in mouse optic nerve after retinal ischemia.** *Neuroimage* 2003;20:1714–22 CrossRef Medline
38. Song SK, Yoshino J, Le TQ, et al. **Demyelination increases radial diffusivity in corpus callosum of mouse brain.** *Neuroimage* 2005;26:132–40 CrossRef Medline
39. Song SK, Sun SW, Ramsbottom MJ, et al. **Dysmyelination revealed through MRI as increased radial (but unchanged axial) diffusion of water.** *Neuroimage* 2002;17:1429–36 CrossRef Medline
40. Wakana S, Jiang H, Nagae-Poetscher LM, et al. **Fiber tract-based atlas of human white matter anatomy.** *Radiology* 2004;230:77–87 CrossRef Medline
41. Gao W, Lin W, Chen Y, et al. **Temporal and spatial development of axonal maturation and myelination of white matter in the developing brain.** *AJNR Am J Neuroradiol* 2009;30:290–96 CrossRef Medline
42. Pierpaoli C, Barnett A, Pajevic S, et al. **Water diffusion changes in Wallerian degeneration and their dependence on white matter architecture.** *Neuroimage* 2001;13(6 Pt 5):1174–85 CrossRef Medline
43. Arfanakis K, Haughton VM, Carew JD, et al. **Diffusion tensor MR imaging in diffuse axonal injury.** *AJNR Am J Neuroradiol* 2002;23:794–802 Medline
44. Smith PM, Jeffery ND. **Histological and ultrastructural analysis of white matter damage after naturally-occurring spinal cord injury.** *Brain Pathol* 2006;16:99–109 CrossRef Medline
45. Budde MD, Frank JA. **Neurite beading is sufficient to decrease the apparent diffusion coefficient after ischemic stroke.** *Proc Natl Acad Sci U S A* 2010;107:14472–77 CrossRef Medline
46. Xie M, Wang Q, Wu TH, et al. **Delayed axonal degeneration in slow Wallerian degeneration mutant mice detected using diffusion tensor imaging.** *Neuroscience* 2011;197:339–47 CrossRef Medline
47. Lober RM, Cho YJ, Tang Y, et al. **Diffusion-weighted MRI derived apparent diffusion coefficient identifies prognostically distinct subgroups of pediatric diffuse intrinsic pontine glioma.** *J Neurooncol* 2014;117:175–82 CrossRef Medline
48. Wagner MW, Bell WR, Kern J, et al. **Diffusion tensor imaging suggests extrapontine extension of pediatric diffuse intrinsic pontine gliomas.** *Eur J Radiol* 2016;85:700–06 CrossRef Medline
49. Hoeft F, Barnea-Goraly N, Haas BW, et al. **More is not always better: Increased fractional anisotropy of superior longitudinal fasciculus associated with poor visuospatial abilities in Williams syndrome.** *J Neurosci* 2007;27:11960–65 CrossRef Medline
50. Thomason ME, Thompson PM. **Diffusion imaging, white matter, and psychopathology.** *Annu Rev Clin Psychol* 2011;7:63–85 CrossRef Medline
51. Budde MD, Kim JH, Liang H-F, et al. **Axonal injury detected by in vivo diffusion tensor imaging correlates with neurological disability in a mouse model of multiple sclerosis.** *NMR Biomed* 2008;21:589–97 CrossRef Medline
52. Nadol JB, Diamond PF, Thornton AR. **Correlation of hearing loss and radiologic dimensions of vestibular schwannomas (acoustic neuromas).** *Am J Otol* 1996;17:312–16 Medline